Influence of Filler Wire and Welding Process to Mitigate the Microsegregation of Alloy C-2000 Using Continuous and Pulsed Current Gas Tungsten Arc Welding Techniques

B. Arulmurugan, D. Balaji, S. Rajkumar, M Kamaraj, V. Mageshwaran, M. Sathishkumar, M. Manikandan, and N. Arivazhagan

This study examines the joining of a 4 mm thick plate of alloy C-2000 by continuous current gas tungsten arc welding (CCGTAW) and pulsed current gas tungsten arc welding (PCGTAW) techniques by using ERNiCrMo-4 (filler-4) and ERNiCrMo-17 (filler-17) as filler wires. This article aims to present a comprehensive structure-property relationship of these welded joints. Weld microstructure was characterized with optical microscope and scanning electron microscope. The results show that PCGTA weldments possess a refined microstructure compared to the CCGTA weldments in both filler wires. Energy-dispersive x-ray spectroscopy study divulged the existence of chromium (Cr)-rich and slight molybdenum (Mo)-rich segregation in the fusion zone interdendritic region of all the four weldments. However, the extent of microsegregation is very low in PCGTA-filler-4 weldment when compared with the other weld joints. Significant grain refinement (8.9 to 9.77%) was observed when shifting the welding mode from CCGTAW to PCGTAW. Weldment produced with PCGTAW-filler-4 offers higher tensile strength (∼4 to 6%), higher toughness (∼5 to 7.5%), and higher hardness (∼3 to 6%) compared to other weldments.

1. Introduction

Alloy C-2000 is a Ni-Cr-Mo-Cu based solid strengthened Ni-based superalloy (Ref 1). The existence of high chromium (Cr) element forms Cr_2O_3 passive film during the oxidizing environment. The presence of molybdenum (Mo) and copper (Cu) enhanced the resistance to sulfuric acid and also in other reducing environments (Ref 2, 3). The presence of 1.6 wt.% Cu and a considerable amount of Mo render lowest corrosion rates for alloy C-2000 among other solid solution strengthened Ni-Cr-Mo based alloys. It replaced conventional alloys C-276 and 625 in many engineering components like heat exchangers, chemical reactors, control valves, and pump components due to outstanding corrosion resistance. Alloy C-2000 is an excellent candidate material in many engineering applications like petroleum refining, power generation, pollution control systems, food treatment, and marine (Ref 3, 4).

In most of the engineering applications, the ability to produce sound weld in solid solution strengthened Ni-Cr-Mo alloys is critical owing to hot cracking (Ref 5). The hot cracking is owing to the potential formation of brittle secondary topologically closed packed (TCP)-phases at the end of solidification (Ref 6). Microsegregation of alloying elements causes the formation of TCP phases in the interdendritic area. The segregation of high Cr content (wt. %) in the interdendritic zone leads to σ phase formation, and similarly higher weight percentage of Mo leads to μ and P-phases formation (Ref 7). It was reported that alloying elements separates preferentially from the liquid during weld solidification owing to their least solubility in the gamma (υ) austenitic matrix. This microsegregation of solute in the interdendritic region resulted in solute less dendrite cores, which can mitigate the mechanical properties and increase the possibility of localized corrosion (Ref 6). Many researchers emphasized the weldability issues in Ni-Cr-Mo family alloys. The following is the related literature reported on various researchers.

Cieslak et al. (Ref 8) studied the hot cracking behavior of three different Ni-based superalloys like C-276, C-4, and C-22 weldments. Among them, alloy C-276 weld was more susceptible to hot cracking due to TCP phases formation, when compared with other alloys. Ragavan et al. (Ref 9) divulged that the aging of alloy C-276 between 650 and 900°C end up with the formation of TCP (μ, M_6C and P) phases. Alloy C-22 weld microstructures were evaluated by Cieslak et al. (Ref 10) and Ogborn et al. (Ref 11). The authors noticed the microsegregation of Mo and W in the interdendritic area of the weld FZ resulted in the poor resistance toward corrosion and reduced ductility. Arul Murugan and Manikandan (Ref 12) and Silva et al. (Ref 13) reported that three TCP secondary phases at the

B. Arulmurugan, D. Balaji, M Kamaraj, and **V. Mageshwaran**, KPR Institute of Engineering and Technology, Coimbatore 641407, India; **S. Rajkumar**, School of Mechanical and Electrochemical Engineering, Institute of Technology, Hawassa University, Hawassa, Ethiopia; **M. Sathishkumar**, School of Mechanical Engineering, Vellore Institute of Technology, Vellore 632014, India; and Department of Mechanical Engineering, Amrita School of Engineering, Amrita Vishwa Vidyapeetham, Chennai 601103, India; and **M. Manikandan** and **N. Arivazhagan**, School of Mechanical Engineering, Vellore Institute of Technology, Vellore 632014, India. Contact e-mail: enggarul@gmail.com.

grain boundary nucleated heterogeneously and could be accountable for the premature failure of the alloy 686 weldment.

The limited studies have been explored on alloy C-2000. Rowe et al. (Ref 14) examined the weldability of alloy C-2000 with the help of a varestraint test. They noticed that the segregation of alloying constituents results in hot cracking. John et al. (Ref 15) examined the microstructure characteristics of the weldments produced by CCGTA and PCGTA welding using autogenous and ERNiCrMo-10 filler. These authors also noticed the accumulation of Cr-rich secondary phases in the weldment.

It is witnessed from the reported literature that elemental segregation of alloying constituents ended with the formation of the secondary phase in alloy C-2000. It is vital to suppress the microsegregation to avoid the secondary phase formation. It can be done by proper selection of the welding method and consumables. The following is some literature discussing promising ways to mitigate secondary phases in nickel-based superalloys in the conventional arc welding technique.

PCGTAW, an excellent variant of CCGTAW, to alleviate hot cracking in most of the nickel-based alloys (Ref 16-18). Farahani et al. (Ref 17) reported that PCGTAW offers superior mechanical properties than CCGTAW, as it allows intermittent variation in arc governing forces, enhanced fluid flow, and continuous changes in the welding pool shape which promote the nucleation of equiaxed grains in alloy 617.

Manikandan et al. (Ref 5, 18) studied the metallurgical characteristics of alloy C-276 welds using CCGTA and PCGTA welding techniques with ERNiCrMo-3 and base metal composition filler-ERNiCrMo-4. The authors also observed that PCGTAW with base metal filler offers negligible microsegregation and excellent mechanical properties. Arul Murugan and Manikandan (Ref 19) evaluated the structure-property relationship of Inconel alloy 686 weldments produced by CCGTA and PCGTA welding technique. They concluded that the refinement in microstructure and improvement in mechanical properties was observed when switching over from CCGTAW to PCGTAW.

As it is evident from the literature, only limited studies are available in welding of alloy C-2000 even though superior properties compared to other Ni-Cr-Mo based superalloys. The current study explores the comparative analysis on the joint fabricated by alloy C-2000 using CCGTA and PCGTA welding with fillers ERNiCrMo-4 (filler-4) and ERNiCrMo-17 (filler-17). Hence, after the filler wire ERNiCrMo-4 will be referred as filler-4 and ERNiCrMo-17 will be referred as filler-17 throughout this study. The filler wires were chosen in such a way that filler-17 is the base metal matching composition filler wire of alloy C-2000. The alloying elements of alloy C-2000 are almost similar to alloy C-276 except the presence of 'Cu' in C-2000. Filler-4 is a matching filler wire of alloy C-276, so this particular filler wire is employed in this study. The presence of 3.3% of W in filler-4 is expected to influence the mechanical properties of alloy C-2000 weldments (Ref 6). This research work focuses on the weld microstructural analysis and mechanical characteristics examination of the alloy C-2000 weldments produced by CCGTAW and PCGTAW. The outcomes of the current study have been helpful for the end-users of alloy C-2000.

2. Materials and Methodology

2.1 Sample Preparation and Welding Process

Alloy C-2000 was acquired in the form of a 4 mm thick plate in hot rolled and solution annealed state. The alloying additions in the procured plate were ascertained by dry spectroscopic test, and the composition of the test result is shown in Table 1. The plates were cut into the size of 130 mm (L) × 55 mm (W) × 4 mm (T) using EDM machine. The plates to be welded were wiped in acetone to remove dust particles, grease or any other impurities. The welding was carried out in the KEMPPI DWE machine in both CCGTA and PCGTAW techniques. Butt joint with a single V-groove of included angle 60º was prepared to accommodate molten metal. Welding was done in 3 passes (root, first and final), in four categories: (i) CCGTAW-filler-4, (ii) PCGTAW-filler-4, (iii) CCGTAW-filler-17 and (iv) PCGTAW-filler-17. Welded plate images are depicted in Fig. 1. Table 2 shows the weld process parameters used in the present study. The process parameters were chosen based on the bead on trials. The cumulative heat supplied to produce CCGTA, and PCGTA weld joints are evaluated by using Eq i, ii and iii.

Cumulative heat supplied to produce CCGTAW is calculated by using Eq i,

$$H_{\text{in}} = \frac{I \times V}{S} \times \eta \text{ in } \left(\frac{\text{kJ}}{\text{mm}}\right) \tag{Eq i}$$

Cumulative heat supplied to produce PCGTAW is estimated by applying Eq ii and iii,

$$\text{Mean Current } I_m = \frac{(I_p \times t_p) + (I_b \times t_b)}{(t_p + t_b)} \text{ in Ampere} \tag{Eq ii}$$

$$H_m = \frac{I_m \times V}{S} \times \eta \text{ in } \left(\frac{\text{kJ}}{\text{mm}}\right) \tag{Eq iii}$$

where, I_P-Pulse current in Ampere (A); I_b-Background current (A); t_p-pulse current duration, in seconds; t_b-Background current duration, in seconds; S-welding speed, in mm/min; V-voltage, V; η-efficiency of the welding process; Arc efficiency (η) is taken as 70% (Ref 20). Heat input values also listed in Table 2.

Welded plates were subjected to non-destructive radiography test to identify the weld defects, and test results confirm the absence of any weld defects. Also, macroanalysis (with dynolite microanalyzer setup) was also performed to identify the defects/cracks in the weldments. Coupons for microstructure analysis were sliced along the longitudinal direction of the weld path with a size of 28 mm × 10 mm × 4 mm. These coupons comprise base metal, HAZ, and fusion zone.

2.2 Metallurgical and Mechanical Characterization

Polishing was done with the help of various grades of emery papers (240-2000 grit), trailed by alumina (Al_2O_3) powder and end with water polish. For getting exact microstructure, the electrolytic etching method was used. Oxalic acid, the etchant used, was prepared with 10 grams of oxalic acid powder and 100 ml of water. The polished workpiece was kept as anode and prepared solution as a cathode, for which a voltage of 1.5 V was supplied for 10 seconds. Figure 3 represents the microstructure of the procured alloy C-2000.

Table 1 Chemical constituent of Hastelloy C-2000 and filler wires

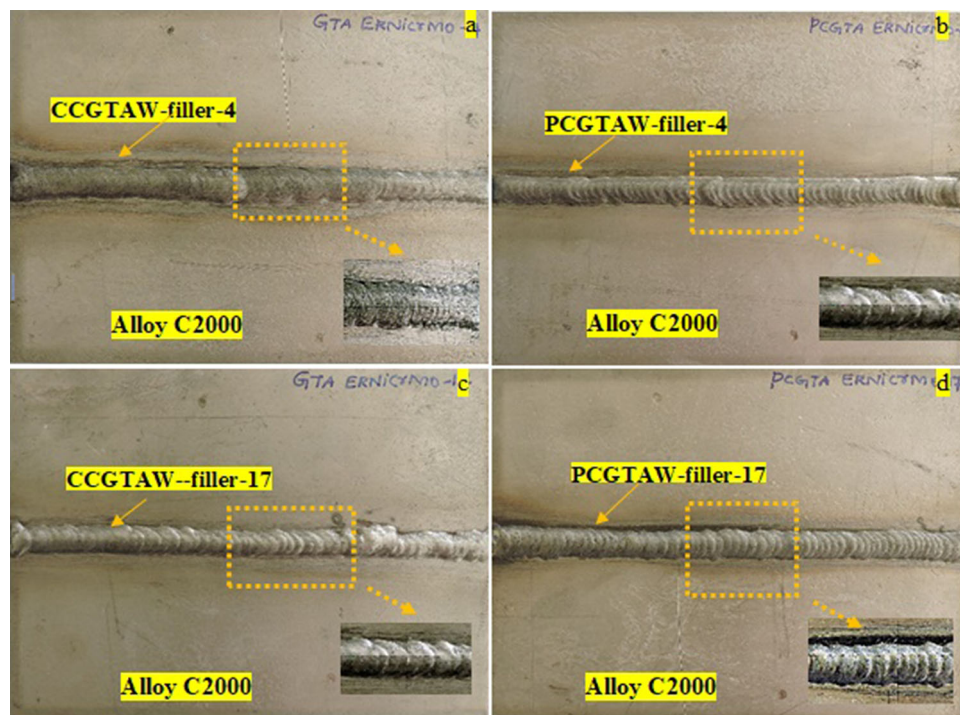| Base/Filler Metal	Chemical constituents (wt.%)						
	Ni	Co	Cr	Mo	Cu	Fe	Others
Hastelloy C-2000	Balance	2	23	16	1.6	3	Mg-0.5, Al-0.5, Si-0.08 , C-0.01
Filler-4	Balance	0.4	16.1	16.1	0.15	5.9	W-3.30, V-0.15, Mn-0.50, C-0.01 P-0.01, Si-0.02, S-0.001
Filler-17	Balance	2	22-24	15-17	1.3-1.9	3	C=0.010, Mn=0.5, P=0.025, S=0.01, Si-0.08, Al-0.5

Fig. 1 Welded plate images of alloy C-2000 fabricated by (a) CCGTAW—filler-4 (b) PCGTAW—filler-4 (c) CCGTAW—filler -17 (d) PCGTAW—filler-17

Table 2 Weld process parameters

Type of welding	Applied Current, A	Applied Voltage, V	Peak Current, A	Background Current, A	Pulse Frequency, Hz	Pulse on Time, %	Welding Speed, s (mm/sec)	Heat Input, kJ/mm
CCGTAW-Filler-4	140	11.11	…	…	…	…	2.048	1.633
CCGTAW-Filler-17	140	12.57	…	…	…	…	1.74	2.189
PCGTAW-Filler-4	…	…	140	98	6	50%	1.833	1.308
PCGTAW-Filler-17	…	…	140	98	6	50%	1.56	1.593

Table 3 Elemental EDS analysis of CCGTAW-Filler-4 (in wt.%)

Welding method	Zone	Ni	Cr	Mo	Fe	Cu	W
CCGTAW-Filler-4	Weld Center Dendritic Core	56±3.1	20.05±1.2	15.08±0.7	4.59±0.5	1.57±0.7	3.4±1.3
	Weld Center Interdendritic region	31.5±7.2	41.15±5.2	17.4±1.6	5.3±1.1	1.49±0.6	3.12±1.6
	Weld interface dendritic core	52.82±4.2	21.62±1.5	15.6±0.7	5.1±0.9	1.51±0.4	3.29±0.8
	Weld interface interdendritic region	33.4±8.3	40.1±4.3	16.8±1.1	4.82±0.7	1.71±0.3	3.1±0.5

Table 4 Elemental EDS analysis of PCGTAW-Filler-4 (in wt.%)

Welding method	Zone	Ni	Cr	Mo	Fe	Cu	W
PCGTAW-Filler-4	Weld Center Dendritic Core	55±4.7	21.7±1.1	15.82±0.9	3.1±0.9	1.58±0.3	2.9±0.8
	Weld Center Interdendritic region	50.1±3.5	23.61±1.8	16.45±0.8	4.53±1	1.42±0.3	3.63±0.9
	Weld interface dendritic core	56.1±2.8	19.9±1.4	14±1.1	5.1±0.9	1.51±0.4	3.3±1.1
	Weld interface interdendritic region	51.4±2.2	23.12±1.8	16.2±0.6	4.41±1.1	1.7±0.2	2.96±0.9

Table 5 Elemental EDS analysis of CCGTAW-Filler-17 (in wt.%)

Welding method	Zone	Ni	Cr	Mo	Fe	Cu
CCGTAW-Filler-17	Weld Center Dendritic Core	54.85±3.5	19.82±3.2	15.1±1.2	4.61±0.9	1.56±0.6
	Weld Center Interdendritic region	34.3±6.2	40.75±2.1	17.9±1.7	3.68±1.1	1.81±0.3
	Weld interface dendritic core	58.39±4.4	21.82±1.9	13.81±1.1	3.97±0.5	1.95±0.2
	Weld interface interdendritic region	41.1±5.1	36.4±4.3	16.3±1.3	4.4±1.4	1.71±0.4

Microstructural features were examined with an optical microscope and SEM/EDS analysis. In order to get reliable result, 50 shots EDS analysis was performed in the welded area and the average value with standard deviation is given in Tables 3, 4, 5, 6. XRD-analysis was carried out to identify the crystalline/grain size (d) in the weld fusion zone. It is calculated by Gaussian method and Scherrer formula. XRD process parameters are taken as follows; Continuous type scan; step size as 0.013°; Range of 2θ from 10.0166° to 89.992°; Scan step time as 48.1950s; Specimen length as 10 mm; measurement temperature as 25°C; Goniometer Radius as 240 mm; distance between focus to divergent slit as 100 mm and generator power set as 30 mA and 45 kV . The tensile test samples were sliced as per ASTM: E8/E-8M13a standard, and to measure the repeatability, three samples were tested in each weldment. This testing was done in INSTRON 8801-UTM Machine. The strain rate employed was 2 mm/minute.

The Charpy test was done on the coupons, which are prepared by ASTM: E23-12C standard. In the center of the weld (cap region), V-notches were cut to facilitate the containment of the impact load only in the FZ. To understand the failure mode in tensile and impact fractured samples, they were characterized using SEM fractography.

Microhardness of weldments was measured with the help of Vickers microhardness tester by following ASTM E384-17 standard. The hardness readings were taken at regular intervals (gap) of 0.25 mm, which covers the entire weld coupon, which consists of a fusion zone, HAZ, and base metal. A typical load of 500 gf and a dwell time of 10sec were applied to measure the hardness values.

3. Results and Discussion

3.1 Macrostructural Investigation

The macrographs of welded samples are shown in Fig. 2(a)–(d). Researchers reported that the inappropriate selection of the filler might lead to the formation of a crack in HAZ and FZ of Ni-Cr-Mo alloys (Ref 5, 6). It is observed from macro-images that no such cracks are present in all the four weldments. Thus, it reflects that the filler wires exploited in this study are well-suited for the base metal. PCGTA weld joints are having narrower weld bead width of 8.4 mm (filler-4) and 8.5 mm (filler-17). However, in case of CCGTAW, width of weld bead is wider for both filler-4 (9.4 mm) and filler-17 (9.7 mm) could be observed. This is due to the cumulative heat inputs (Table 2) supplied during the CCGTAW, which is significantly higher (1.663 and 2.189 kJ/mm) than PCGTAW (1.308 and 1.593 kJ/mm) method with respect to filler-4 and filler-17. Further, it is noticed that the proper steady flow of weld pool and full depth of penetration is achieved in all cases. It shows that the weld bead profile governing forces (Lorentz and buoyancy force) and stresses (Shear stress produced by plasma jet and shear stress made by Marangoni convection) are well balanced. But the magnitude of overall heat input is low in PCGTAW, which is due to the minimal temperature at the weld pool center, and it induces reduced shear stress by Marangoni convection as well as by plasma jet when compared to CCGTAW (Ref 21). It might result in an adequate heat supply per unit volume, which subsequently offers a lower bead width and higher depth of penetration in PCGTAW. The electromagnetism, buoyancy, surface tension increased the weld pool circulation. This promotes interdendritic fluid flow. The phenomenon of con-

Table 6 Elemental EDS analysis of PCGTAW-Filler-17 (in wt.%)

Welding method	Zone	Ni	Cr	Mo	Fe	Cu
PCGTAW-Filler-17	Weld Center Dendritic Core	56.15±3.45	21.4±2.1	15.58±1.3	4.11±0.7	1.69±0.3
	Weld Center Interdendritic region	51.1±4.7	26.4±1.1	16.4±0.9	4.15±0.8	1.72±0.3
	Weld interface dendritic core	56.2±3.1	21.2±1.4	15.1±1.6	4.2±1.1	1.61±0.4
	Weld interface interdendritic region	52.72±3.8	22.3±1.7	16.4±0.9	4.3±0.9	1.76±0.4
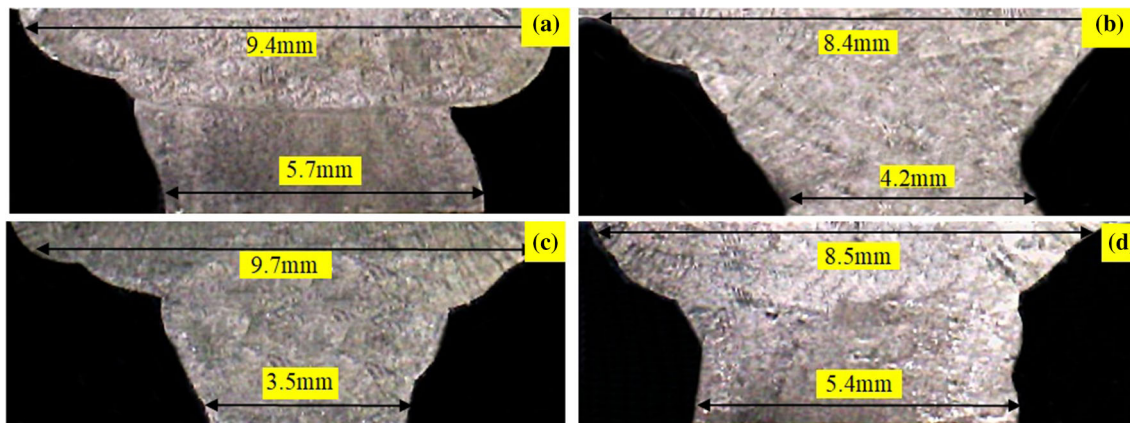
Fig. 2 Macro-examination images of alloy C-2000 weld joints fabricated by (a) CCGTAW—filler 4 (b) PCGTAW—filler -4 (c) CCGTAW—filler-17 (d) PCGTAW – filler-17

vective heat transfer mainly affects the penetration and structure of the weld bead. The significant effect of convective transfer is not identified in GTAW. But the repeated occurrence of melting and solidification increased the convective heat transfer at the solid-liquid region of PCGTAW. This results in rapid solidification due to faster heat dissipation.

During solidification, the shrinkage of molten pool along with increased solid fraction arrest the fluid flow and results in reduced velocity. In addition, during pulsed current conditions, the electromagnetic forces are maximum in the molten pool. In pulsed current method, the driving forces control the convection occurring in the weld pool. Besides, the arc force is greater by shape factor times for PCGTAW. The radiation intensity is almost similar for both PCGTAW and GTAW. But the radiation losses are minimized at high-frequency PCGTAW. This results in enhanced electromagnetic forces and weld pool stirring. Hence, the weld pool depth of penetration along with depth-to-width ratio is improved during weld pool stirring. During PCGTAW, the changes of arc force vigorously affect the physical movement of molten pool. As stated by Saedi and Unkel (Ref 22), the electromagnetic forces are higher during the current pulsing stage, which strongly stimulates the electromagnetic spinning in the weld center, resulting in narrow weld beads (Fig. 2).

3.2 Microstructure Investigation

3.2.1 CCGTA and PCGTA Welding with Filler-4. Figure 3 represents the microstructure of the alloy C-2000 plate in the as-received state. The microstructure of the parent alloy contains annealing twins' structures near the grain boundaries. Annealing twins were formed during the solution treatment.

Figure 4 and 5 shows the OM images of the CCGTA and PCGTA welds made with filler-4. The fusion zone microstruc-

Fig. 3 Optical microstructure of alloy C-2000 base metal

ture is shown in Fig. 4(a), and it consists of cellular and columnar dendrites. Figure 4(b) shows the interface region, which contains planar near the fusion boundary and cellular structure when moving toward the weld center. The composition of various grains in the weld microstructure is strongly governed by the temperature gradient (G) and growth rate (R), as proposed by DuPont (Ref 23). At high G/R levels, the actual transformation of the planar to the cellular structure will take place; furthermore, as the G/R declines, microstructural evolution shifts from cellular structure to columnar and then to the equiaxed dendritic structure. Due to the continuous supply of heat in CCGTAW mode, a large amount of heat is transferred to base metal, which could be observed from a wider HAZ of (average size) 129.7 μm. The grain coarsening is noticed in the
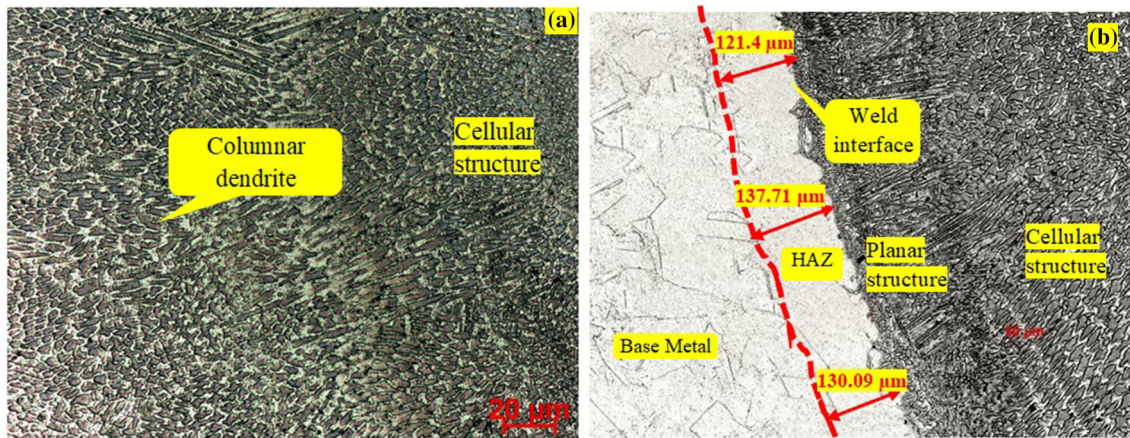
Fig. 4 Optical microstructure image of alloy C-2000 weld made by CCGTAW-filler-4 (a) FZ and (b) Weld Interface
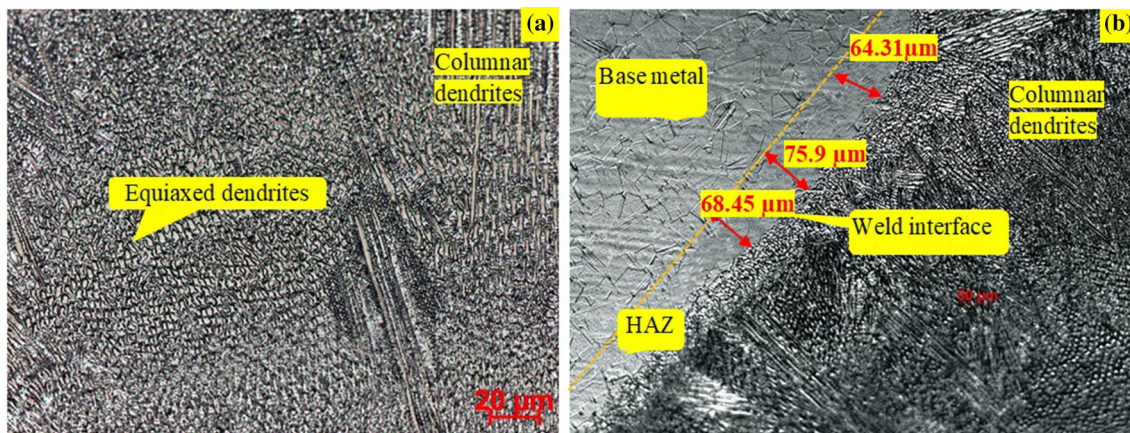

Fig. 5 Optical microstructure image of alloy C-2000 weld made by PCGTAW-filler-4. (a) FZ and (b) Weld Interface

HAZ next to the fusion boundary. Higher input is also attributed to grain coarsening in this case.

Figure 5(a) and (b) shows the microstructure of the weld center and interface of PCGTA-filler-4 weldment. Weld center has been observed with the presence of equiaxed grains and few columnar grains while the weld interface shows columnar dendrite structure. It confirms the columnar to equiaxed transition. Welding current will be fluctuating between peak and background ranges during current pulsing. At the peak current cycle, the melting of the faying surface takes place, and the heat dissipation takes place during the background current cycle. This frequent cyclic change of the energy supply to the weld pool triggers thermal variations, which offers multiple instantaneous solidifications during the PCGTA welding. This significantly declines the G/R ratio creating a favorable condition to form fine equiaxed grains.

The HAZ size is significantly less (69.55 μm) when compared with CCGTAW-filler-4. In PCGTAW, the heat needed to melt the base metal (BM) is only applied for a short period at peak current pulses. So, subsequent (background) cycle helps in heat dissipation through the base material, contributing to a smaller HAZ (Ref 24), which is not probable in CCGTAW.

3.2.2 CCGTA and PCGTA Welding with Filler-17. Figure 6 and 7 depicts the optical microscopic image of the weld joints made with PCGTAW-filler-17. Figure 6(a) shows the presence of cellular as well as columnar dendrites in the weld fusion zone. Weld interface is observed in Fig. 6(b), and it also confirms the planar to cellular transition. The HAZ is wider (average size = 159.7 μm) than in previous cases, which is due to a large amount of heat supplied (2.18 kJ/mm).

Figure 7(a) shows the fusion zone of PCGTAW with the filler-17. The equiaxed dendrites were again observed along with columnar dendrites. Figure 7(b) shows the weld interface with columnar dendrites predominantly. This is because of the incomplete columnar to equiaxed transition. The HAZ is also visible with an average size of 103.75 μm, which is comparatively lower than the CCGTAW-filler-17 case.

The weld microstructure of CCGTAW predominately contains the cellular structure and columnar dendrites. In contrast, PCGTAW prevails with fine equiaxed grains in FZ and columnar dendrites near the weld interface.

CCGTA weld microstructures were coarser than PCGTA welds. The cooling/solidification rate is normally lower in CCGTAW. The constant supply of heat, in this case, never permits any provision for heat dissipation during welding, resulting in the coarser microstructure. Inherent slow cooling rate, steep temperature gradient and higher diffusion rate in CCGTA welding may not retard the grain growth and do not
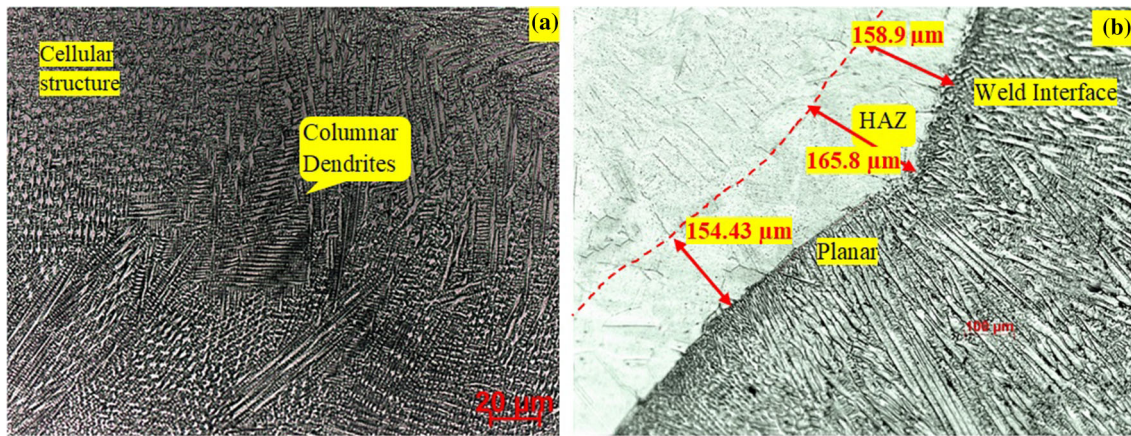
Fig. 6 Optical microstructure image of alloy C-2000 weld made by CCGTAW-filler-17 (a) FZ and (b) Weld Interface
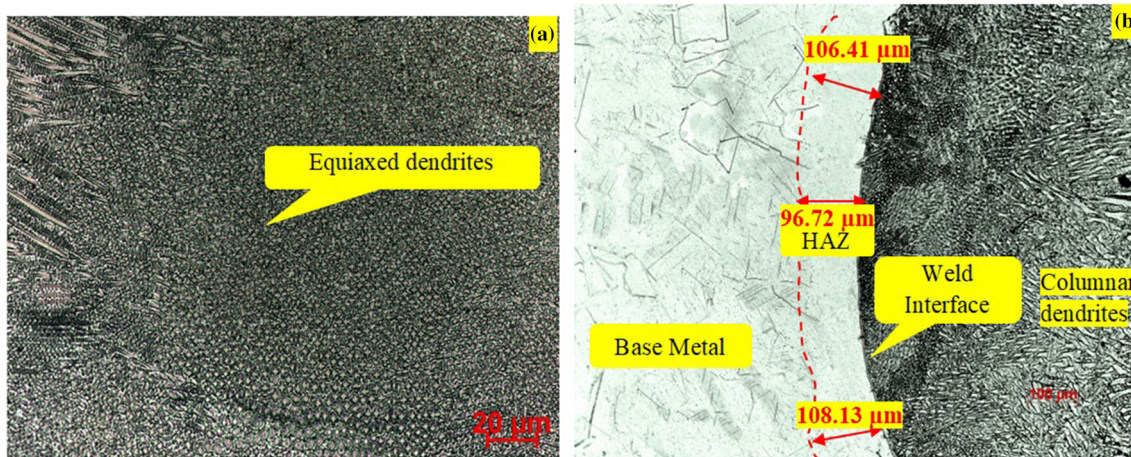

Fig. 7 Optical microstructure image of alloy C-2000 weld made by PCGTAW-filler-17. (a) FZ and (b) Weld Interface

permit the fresh grains to form. Also, the grain that is part of the welding process only grows inside, leading to the formation of a columnar and cellular microstructure (Ref 17). Hence, only due to grain growth, the columnar and cellular dendritic microstructure is formed.

In the PCGTA welding method, metal melting takes place only during peak current (I_P) cycle. At the time of background (I_B) current supply, solidification of molten metal will be taking place, which supports the fresh grain formation in the weld region. As the current rises in the consecutive cycle, new grain nucleation is stopped, and re-melting of existing grain occur (Ref 12). The prolonged occurrence of these cycles results in the nucleation of new grains and the growth of existing grains. Consequently, the grain growth, along with the nucleation of grains, rises in the small area, resulting in the refined weld microstructure. As pointed out by Sindo kou (Ref 25), constitutional supercooling will also facilitate the formation of equiaxed grains, which naturally exists in PCGTAW. Further, equiaxed grains significantly reduce the risk of solidification cracking and enhance the ductility, fracture toughness, and other mechanical properties. During solidification, the materials tend to develop directional properties, which give rise to different properties in a different direction. That is, the mechanical properties will be different in different coordinated axes of X, Y, and Z. This is the major limitation in anisotropic columnar dendrites. However, if equiaxed grain structure is

obtained in the weld microstructure, the mechanical properties in all the three directions will be equal, maintains isotropic characteristics. As well as there is an equal amount of dendrite arm spacing in all three directions. Further, fine equiaxed grains can more quickly deform to withstand contraction strains because they are more ductile than columnar grains.

3.3 SEM/EDAX Analysis

3.3.1 CCGTA and PCGTA Welding with Filler-4. Figure 8 and 9 denotes the SEM/EDS examination of the weld joints produced by (CCGTAW and PCGTAW) filler-4. Figure 8(a) depicts the SEM photograph of the weld center, and Fig. 8(b) denotes the SEM photograph of the weld interface. Both areas contain columnar and cellular grain structure along with the secondary phases (white-colored particles) distributed all over. Figure 8(i) and (ii) depicts the EDS image of the dendritic core and the interdendritic zone of the weld center. Table 3 shows the salient elemental values consolidation in different areas of CCGTA-filler-4 weld joint in weight percentage (wt. %). Figure 8(i) and (ii) and Table 3 show that the interdendritic area is augmented with Cr and depleted Ni content related to the dendritic core. Slightly Mo content is also enriched in this region. Figure 8(iii) and (iv) depicts EDS analysis of the weld interface, where the results are observed to be the same as the weld center.
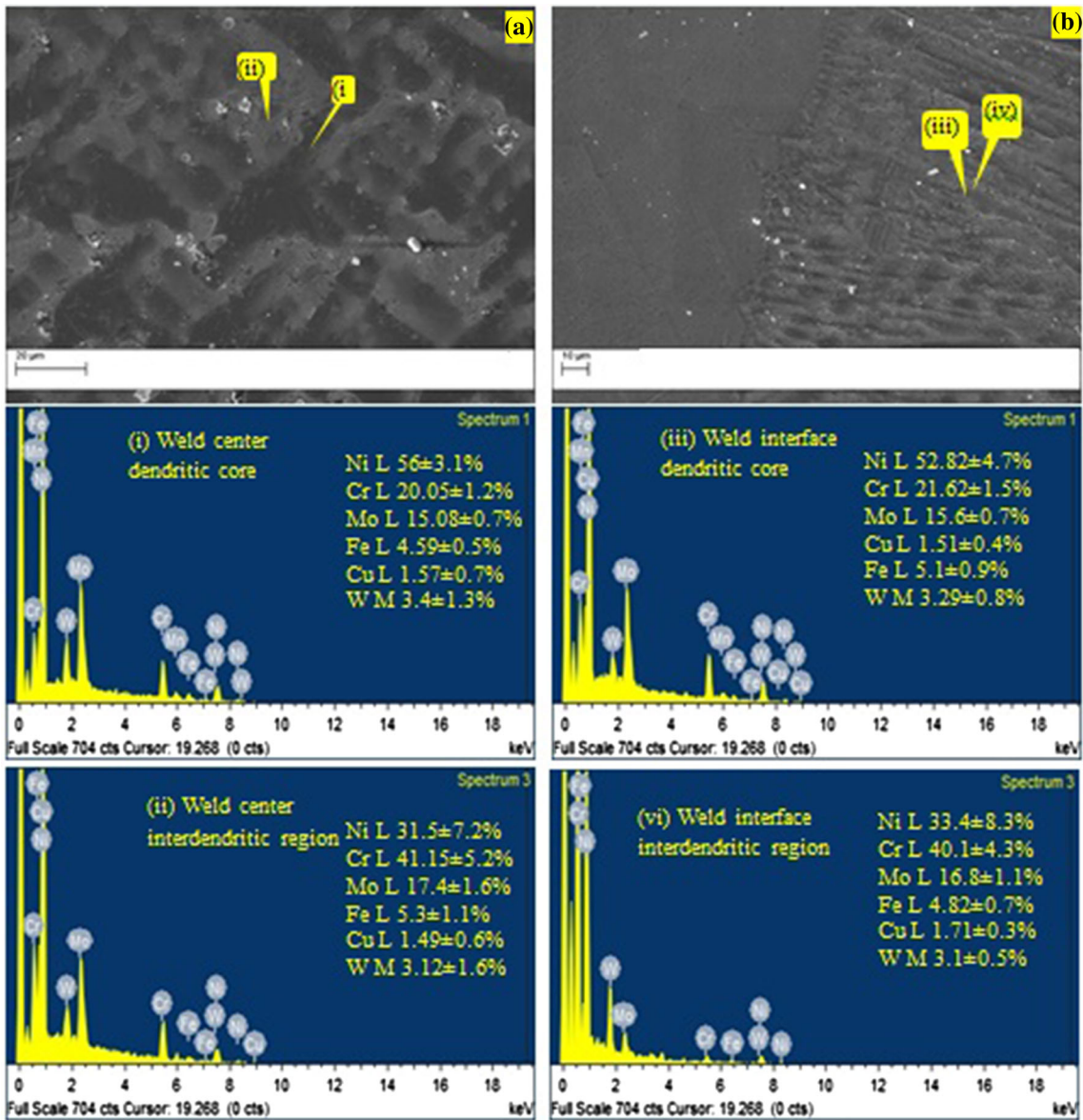
Fig. 8 SEM examination of alloy C-2000 welded with CCGTAW-filler-4 (a) Weld Center (WC) (b) Weld Interface (WI) and EDS analysis of (i) WC dendritic core (ii) WC interdendritic region (iii) WI dendritic core (iv) WI interdendritic region

Slower cooling CCGTAW (due to higher input) gives enough time to segregate the alloying elements in the interdendritic region and make a favorable situation to form Cr- and Mo-rich brittle secondary phases (Ref 12).

Figure 9(a) and (b) displays the SEM images of the PCGTA-filler-4 weld center and interface, respectively. Table 4 consolidates the salient elemental values in different areas of this weldment. Figure 9(a) shows the SEM micrograph of the weld center, which contains a fine equiaxed dendrite. The micrograph shows the very minimum (almost negligible) distribution of secondary phases in the interdendritic area. Figure 9(i) and (ii) denotes the EDS image of the dendritic core and interdendritic area of the weld center. In this, the interdendritic area comprises of a slightly higher content of Cr and Mo, and depleted Ni content. In the weld interface region, similar observations are made (Fig. 9 iii and iv). As compared to CCGTAW, the segregation of Cr and Mo is suppressed in PCGTAW. Inherent rapid cooling rate and less activated

diffusion of PCGTAW do not give enough time to segregate the alloying elements in the FZ—interdendritic region.

3.3.2 CCGTA and PCGTA Welding with Filler-17. Figure 10(a) and (b) depicts the SEM image of weld regions with the CCGTAW-filler-17. The fusion zone contains cellular structure (Fig. 10a), and columnar dendrites are visible in the interface region (Fig. 10b). Both weld center and interface areas were decorated with secondary phase precipitates.

Figure 10(i) and (ii) shows the EDS image of the FZ weld center dendritic core and interdendritic area of the CCGTAW-filler-17. Table 5 clearly shows that the interdendritic area is augmented with Cr & Mo contents, but depleted Ni content in the dendritic core. Weld interface zone is also characterized with same observations (Fig. 10iii and iv).

Figure 11(a) and (b) shows the SEM image of the PCGTAW-filler-17 weld center and interface zone. Table 6 consolidates the elemental values in different areas of this weldment. The interface consists of columnar dendrites (Fig. 11b) and also contains lesser brittle secondary phases
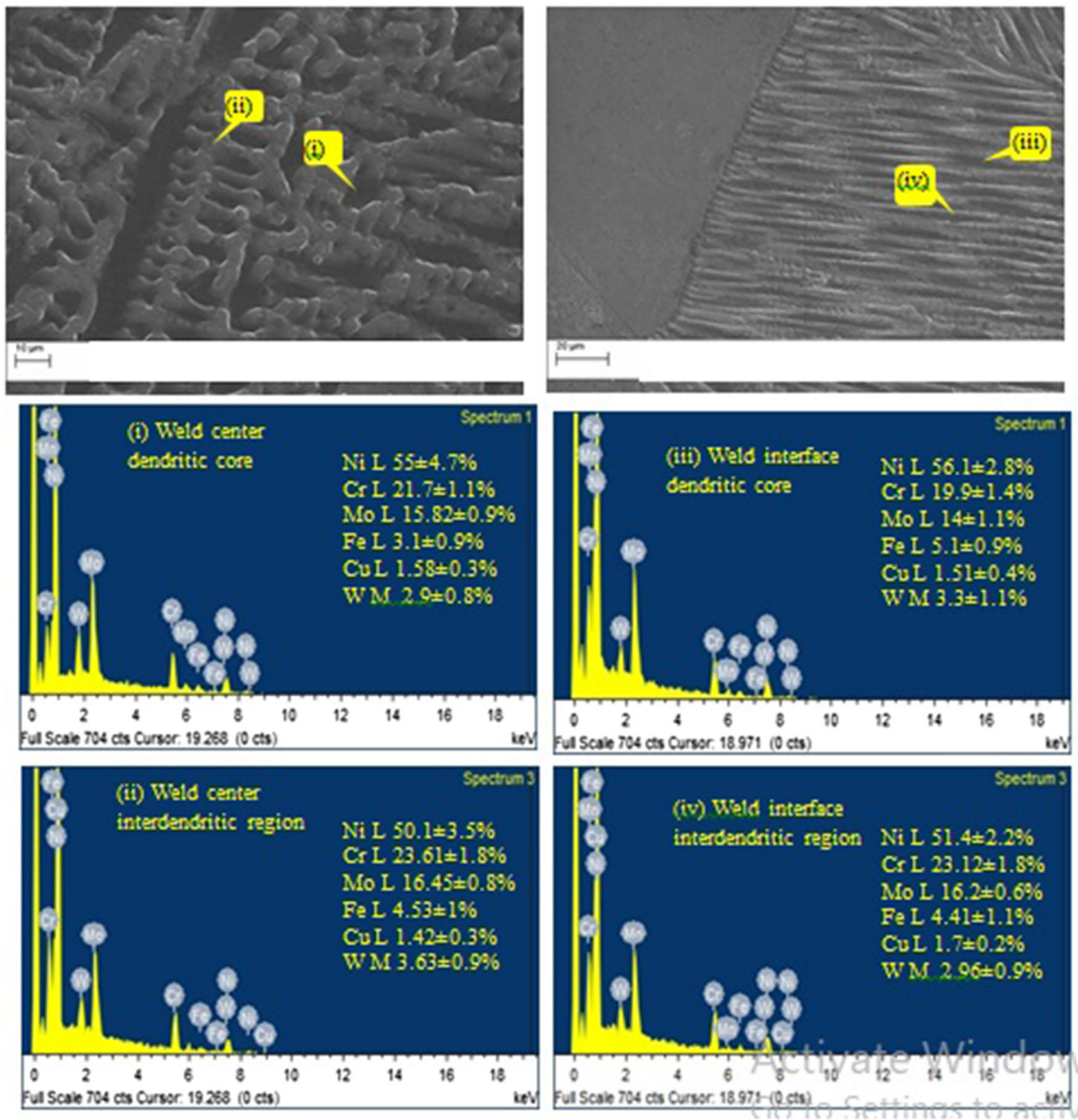
Fig. 9 SEM examination of alloy C-2000 welded with PCGTAW-filler-4 (a) Weld Center (WC) (b) Weld Interface (WI) and EDS analysis of (i) WC dendritic core (ii) WC interdendritic region (iii) WI dendritic core (iv) WI interdendritic region

but not as much in CCGTAW cases. Figure 11(i) and (iv) denotes the EDS point analysis of this case. Even here, the slight Cr augmentation and Ni impoverishment could be observed. In the welding interface region, similar observations were also observed (Fig. 11iii and iv).

The SEM micrographs also demonstrate that the absence of microcrack in the FZ and HAZ in all the above cases. The result is in line with the analysis of the macrostructure. It is observed from Table (3, 4, 5, 6) that FZ—dendritic core—interdendritic zone is augmented with Cr, the slight rise in Mo and impoverished Ni content, except in the PCGTAW-filler-4 case.

From higher magnification of CCGTAW - SEM images (Fig. 8a–b and 10a–b), it is evidently seen that secondary phases are present in interdendritic zones. In CCGTA welding, severe microsegregation is owing to the high (G/R) ratio and slow cooling rate, which favored the formation of secondary phases. In the case of PCGTA (Fig. 9a–b and 11a–b) welding, secondary phases could be observed, but they were considered

lesser than CCGTAW. Rapid cooling rate, less (G/R) ratio, and less diffusion rate in PCGTA welding do not permit the segregation of alloying elements, which mitigates the secondary phases formation. It can be observed that the segregation of Cr has increased in all the regions but very less in PCGTAW-filler-4 comparatively. This shows that the potential formation of the chromium-rich phase is marginally low in this case.

It is clear from Table 1 that the addition of the alloy elements by the filler-17 to the weld pool is higher compared with the other filler-4. More inclusion of alloying elements, especially Cr, by filler-17, exceeds the solubility limit at the time of eutectic reaction and get separated in the interdendritic region of PCGTA-filler-17 welding. Although it is a matching filler of alloy C-2000, it causes moderately quotable microsegregation. Specifically, in the case of PCGTAW-filler-4, mild microsegregation is noticed, but it is very minimal compared with other counterparts. This may be attributed to the optimal
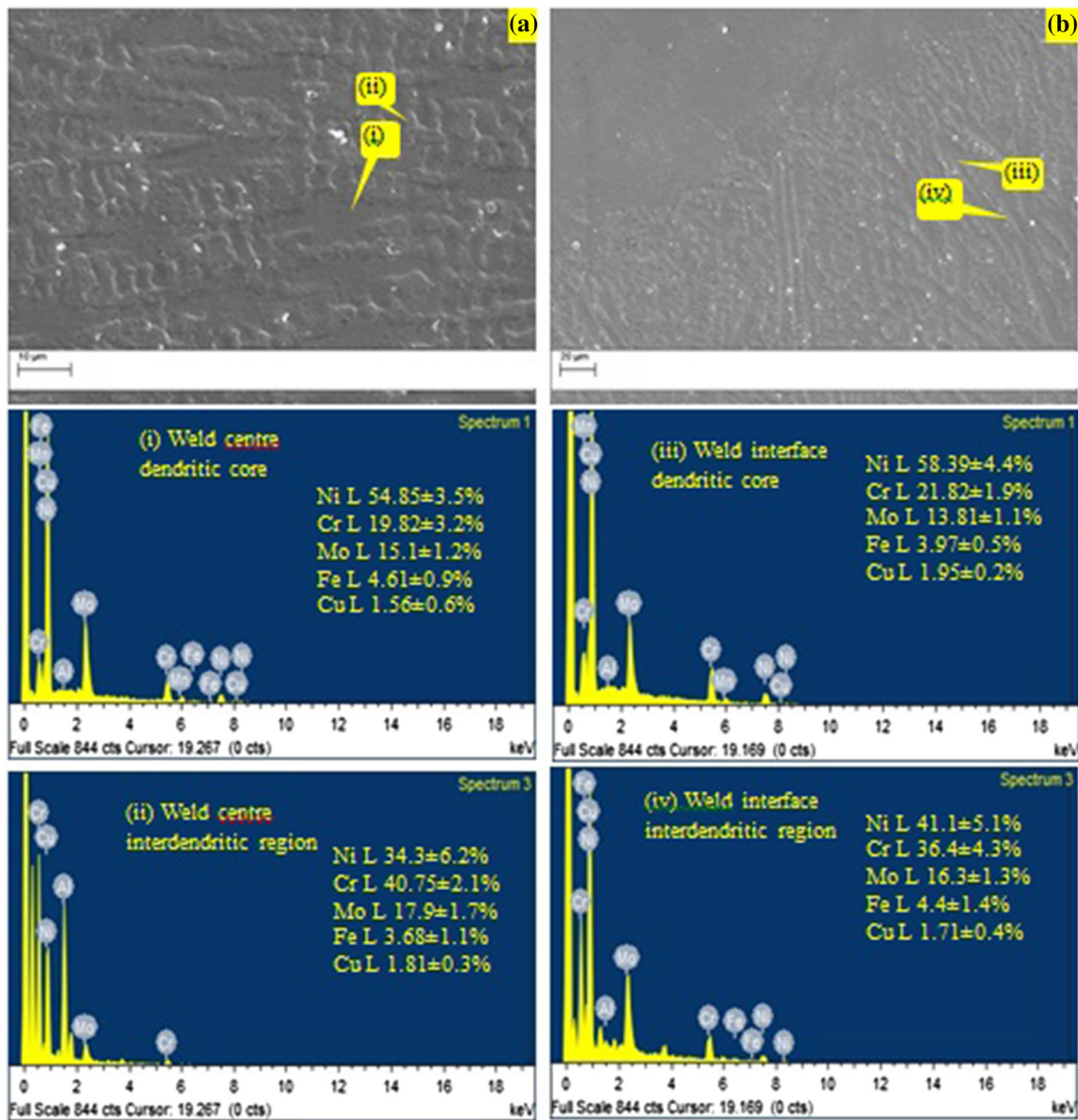
Fig. 10 SEM examination of alloy C-2000 welded with CCGTAW-filler-17 (a) Weld Center (WC) (b) Weld Interface (WI) and EDS analysis of (i) WC dendritic core (ii) WC interdendritic region (iii) WI dendritic core (iv) WI interdendritic region

supply of solute elements by the filler-4, which ensures good solubility and reduced the microsegregation.

In the present investigation, in addition to the semi-quantitative EDS analysis, the Scheil equation is also used to compute the microsegregation of alloy elements. Many authors utilized this equation to access the microsegregation in Ni-Cr-Mo alloys (Ref 12, 19) and is shown in Eq iv.

$$\text{Distribution Coefficient (k)} = \frac{C_{\text{core}}}{C_{\text{o}}}$$

$$= \frac{\text{Dendrite core elemental level}}{\text{Elemental level in the nominal composition of the alloy}}$$

$$\text{(Eq iv)}$$

The intensity of microsegregation by the alloy elements during solidification is quantified by the distribution coefficient. If the value of 'k' < 1, the probability of greater segregation in the interdendritic zone increases and makes a favorable situation to form the brittle secondary phases. However, if the value of 'k' > 1, the dendrite core is more segregated (Ref 19, 26). Table 7 represents the distribution coefficient (k) values for all weldments employed in this study. It indicates that the 'k' value of Cr and Mo is less than one, which noticeably specifies the acute segregation in both CCGTAW weld's interdendritic region. But the 'k' value of Cr and Mo is almost one for PCGTA welding, and this shows a minimum secondary phase formation.

In addition, solid solution strengthened alloys gained greater mechanical properties and excellent corrosion resistance in aggressive environments by the addition of alloying elements. Different alloying elements cause solid solution strengthening effect and produce much higher properties according to Hume-Rothery rule. Once these alloying additions exceed the solubility limit, they cause microsegregation. Dupont et al. (Ref 6) emphasized that even though Ni-Cr-Mo alloys were designed to be single phase, but if composition exceeds the
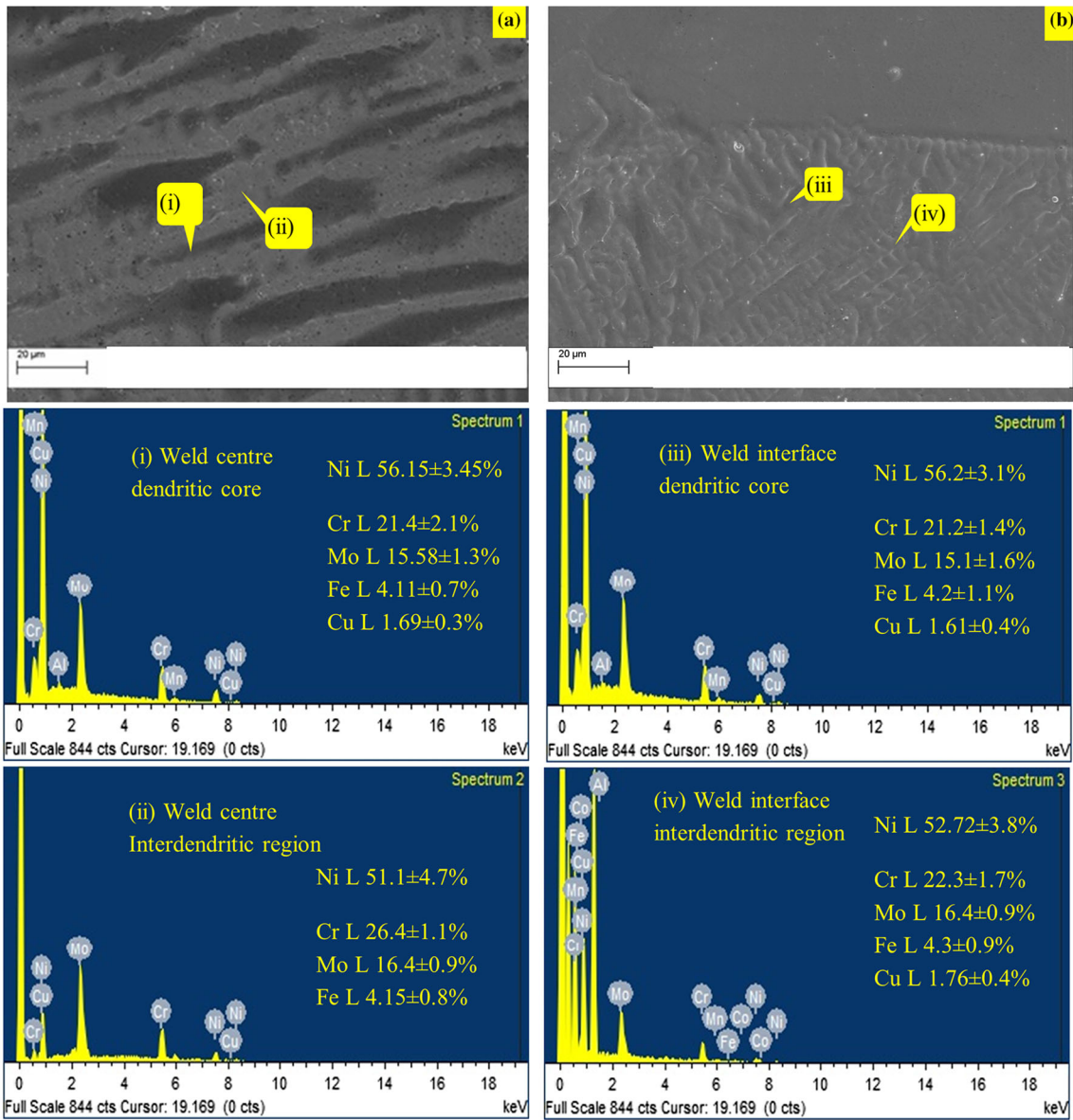
Fig. 11 SEM examination of alloy C-2000 welded with PCGTAW-filler-17 (a) Weld Center (WC) (b)Weld Interface (WI) and EDS analysis of (i) WC dendritic core (ii) WC interdendritic region (iii) WI dendritic core (iv) WI interdendritic region

Table 7 Distribution coefficient (k) values of alloy C-2000 weldments

Type of welding	Ni	Cr	Mo	Fe	Cu
CCGTAW-Filler-4	1.00	0.91	0.94	1.53	0.98
PCGTAW-Filler-4	0.99	0.99	0.99	1.03	0.99
CCGTAW-Filler-17	0.98	0.90	0.94	1.53	0.98
PCGTAW-Filler-17	1.00	0.97	0.97	1.37	1.05

solubility limit, given adequate time to expose at high temperatures, can form a different brittle secondary phase. During the weld solidification of Ni-Cr-Mo alloy joining, segregation is unavoidable, since W and Mo solidify (higher melting elements) before Ni and Cr owing to lower melting temperature elements.

For example, secondary phase formation in different solid solution strengthened nickel alloys is given in Table 8. Key mechanism required to control microsegregation is higher/rapid cooling rates and short solidification time. These two factors effectively achieved in PCGTA welding which offer refined microstructure, reduced elemental microsegregation, absence of brittle secondary phases also surges mechanical and corrosion properties in different nickel-based alloys. Farahani et al. (Ref 17) examined the weld microstructure and mechanical properties of Inconel 617 made by GTAW and PCGTAW process. The authors noticed that PCGTAW welds came out with finer equiaxed grains which offer higher mechanical properties than GTAW process. The authors noted the smaller HAZ and less microsegregation in the PCGTAW. Similarly, different researchers noticed suppress in microsegregation and enhancement in properties by employing PCGTA welding in different nickel-based alloys like alloy 600 (Ref 16), C-276 (Ref 18), alloy 686 (Ref 19), alloy 617 (Ref 26) and alloy 718 (Ref 27).

Table 8 Secondary phase formation in different solid solution strengthened nickel alloys

Alloy	Type of secondary phase	Reason for existence
Alloy 625	Laves and Delta	Segregation of Niobium
Alloy 600	M_6C	Segregation of Chromium
Alloy 617	$M_{23}C_6$	Segregation of Chromium and Molybdenum
Alloy C-22	σ , P and μ	Segregation of Chromium and Molybdenum
Alloy C-276	P and μ	Segregation of Molybdenum
Alloy 686	σ , P and μ	Segregation of Chromium and Molybdenum

Table 9 Measurement of average dendrite arm spacing and grain size

Type of welding	Average Primary Dendrite Arm Spacing, μm	Average Secondary Dendrite Arm Spacing, μm	Average grain size, nm
CCGTAW-Filler-4	12.63	2.98	293.7
PCGTAW-Filler-4	5.12	2.03	267.5
CCGTAW-Filler-17	10.85	3.58	305
PCGTAW-Filler-17	5.97	2.43	275.2

3.4 XRD Analysis

XRD analysis is performed on the C-2000 welded samples in order to measure grain size (d). It is calculated by Gaussian method and the Scherrer formula (v).

$$d = \frac{k\lambda}{\beta \cos\theta} \text{ in (nm)} \qquad \text{(Eq v)}$$

whereas d'—average grain size (in nm), λ- wavelength of x-ray in m (1.54×10^{-10} m), β - the diffraction line expansion at full width half maximum (FWHM) intensity, which is taken from XRD (in radiant), 'k'- dimensionless shape factor = 0.94 and θ- the angle of diffraction (in degree).

The grain size (d) for the CCGTAW-filler-4 approach is 293.7 nm, and for PCTGAW-filler-4 mode, its value is 267.5 nm. Similarly, the d' value for CCGTAW-filler-17 case is 305 nm, and PCTGAW-filler-17 is 275.2 nm. When the welding mode changes from CCGTA to PCGTA welding, the overall percentage reduction/ grain refinement in the PCGTA weld is 8.9 % for the filler-4 case and 9.77% for the filler-17 case. It indicates that the significant refinement of grain takes place when shifting from CCGTA to PCGTA welding. It also favors mechanical properties enhancement. Detailed Metallographic characteristics of the intermetallic elements present in these weldments will be explored in future study with TEM analysis.

Microstructural features like primary dendritic arm spacing (PDAS) and secondary dendritic arm spacing (SDAS) are measured from Fig. 4, 5, 6, 7, using ImageJ software and the results are listed in Table 9. This table clearly indicates that both PDAS and SDAS are significantly lower for the weldment made with PCGTAW-filler-4. Effective cooling rate inherent in PCGTA made these favorable dendritic features.

3.5 Tensile Test Examination

Tensile test results of C-2000 weldments are shown in Table 10. This table also contains base metal and filler materials tensile properties for comparison. Figure 12(a)–(d) displays the tensile failure of weldments, and the Figure clearly shows that the tensile fracture (sample broken) happens at the FZ in all cases. Microsegregation and formation of brittle secondary phases are responsible for the fracture in the weld FZ. Dupont et al. (Ref 6) described that the mechanical characteristics of Ni-based alloy weld joints were decreased by the potential formation of brittle secondary phases. The results of the tensile test show that PCGTA weld joints have higher tensile properties than those of CCGTA welds.

There was a reduction in ultimate tensile strength and ductility noted in all cases when correlated with a base metal. The presence of more Cr-rich secondary phases in FZ is the main cause for the reduction in ultimate tensile strength (UTS) than base metal strength. This has also been supported by OM and SEM microstructure studies. Table 10 shows that PCGTAW-filler-4 weld has the highest UTS and ductility compared with both CCGTAW cases and PCGTAW-filler-17 welded specimens since it has lower microsegregation.

Similarly, the richer components of alloying elements in filler-4 (particularly W=3.3%) exhibited a solid solution strengthening effect. Tungsten is having a considerably bigger atomic radius than Ni (10 percent) and also a different crystal structure (BCC) showing a minimum tendency to segregate in Ni alloys. This makes 'W' an excellent solid solution strengthener (Ref 6) and gave the weld zone greater strength than the other counterparts. Weldment produced with PCGTAW-filler-4 offers greater ultimate tensile strength ($\sim$ 4% to 6%) and better ductility ($\sim$ 0.5% to 6.9 %), compared to other weldments. The existence of the Cr-rich phase is a factor for the decrease in ductility of CCGTA welds relative to PCGTA welds. The improvement in UTS and elongation in PCGTA welding is also attributed to 8.9% and 9.77% reduction of grain size relative to CCGTA welding. Further shorter PDAS and SDAS (Table 9) supported more number of fine grains per unit volume which enhances the tensile and other mechanical properties. These results were in coincidence with the SEM/EDS study, as discussed in Section 3.3. Analysis of tensile fractography (Fig. 13a–d) demonstrates the coalescence of micro-voids and shallow dimples dispersed over the fibrous fractured zone. The surface of the fracture is distinguished by the presence of ductile dimples (microvoid coalescence), ductile tearing ridges,

Table 10 Tensile test results of alloy C-2000 weldments

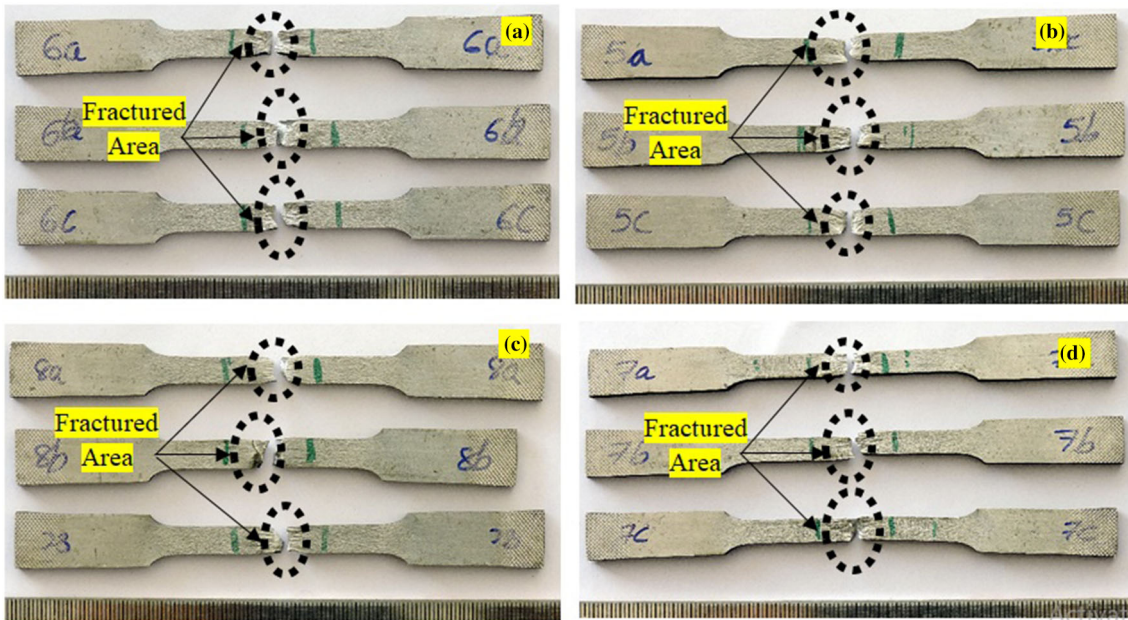| Welding Method	UTS, MPa	Average UTS, MPa	% of Elongation	Average % of Elongation	Fractured Zone	% decrease from base metal
Base Metal	1046	1046	78.12	78.12	…	…
ERNiCrMo-4 filler	744.6	744.6	42	42	…	…
ERNiCrMo-17 filler	735	735	22	22	…	…
CCGTAW-Filler-4	942	944±21	46.90757	48.46±1.7	Fractured at FZ	9.75
	920		48.11753			
	963		50.38803			
PCGTAW-Filler-4	1007	1004±26	51.57586	51.5±1.2	Fractured at FZ	4
	1030		52.68199			
	975		50.27383			
CCGTAW-Filler-17	978	963±17	50.72674	49.17±2.5	Fractured at FZ	7.9
	944		46.2887			
	968		50.4966			
PCGTAW-Filler-17	974	988±21	51.0521	51.22±0.6	Fractured at FZ	5.5
	986		51.93616			
	1005		50.69455			

Fig. 12 Images of tensile fracture samples of alloy C-2000 weldments made by (a) CCGTAW-filler-4 (b) PCGTAW-filler-4 (c) CCGTAW-filler-17 (d) PCGTAW-filler-17

and fewer cleavage facets. These facts confirm the ductile failure mode for all four weld joints (Ref 28, 29). In all fractography samples, the dimension of the ductile dimple is heterogeneous in nature. Furthermore, results (Fig. 14i–iv) of the EDS on the tensile broken surface of all weld samples support the microsegregation of Cr-rich elements, which mainly admits failure occurred in the fusion region.

3.6 Impact Test Examination

The impact test results of all weld joints employed in this study are listed in Table 11. The impact test images are shown in Fig. 15(a)–(d). Impact study on the alloy C-2000 welding shows (Table 11) that the impact strength of PCGTAW-filler-4 weld joint (60.3 J) is better than CCGTA welding (57 J and 55.4 J). The CCGTAW-filler-17 impact strength value is least among the other welds involved in this study and is due to the severe microsegregation. The results of the impact study show that the weld joint prepared with PCGTAW -filler-4 filler exhibited higher (∼5% to 7.5%) toughness when compared to other weldments. Further, the addition of more W (3.3%) by the filler-4 also improves impact strength due to solid solution strengthening effect (Ref 6). The refined microstructure (with small PDAS, SDAS and grain size) and least microsegregation
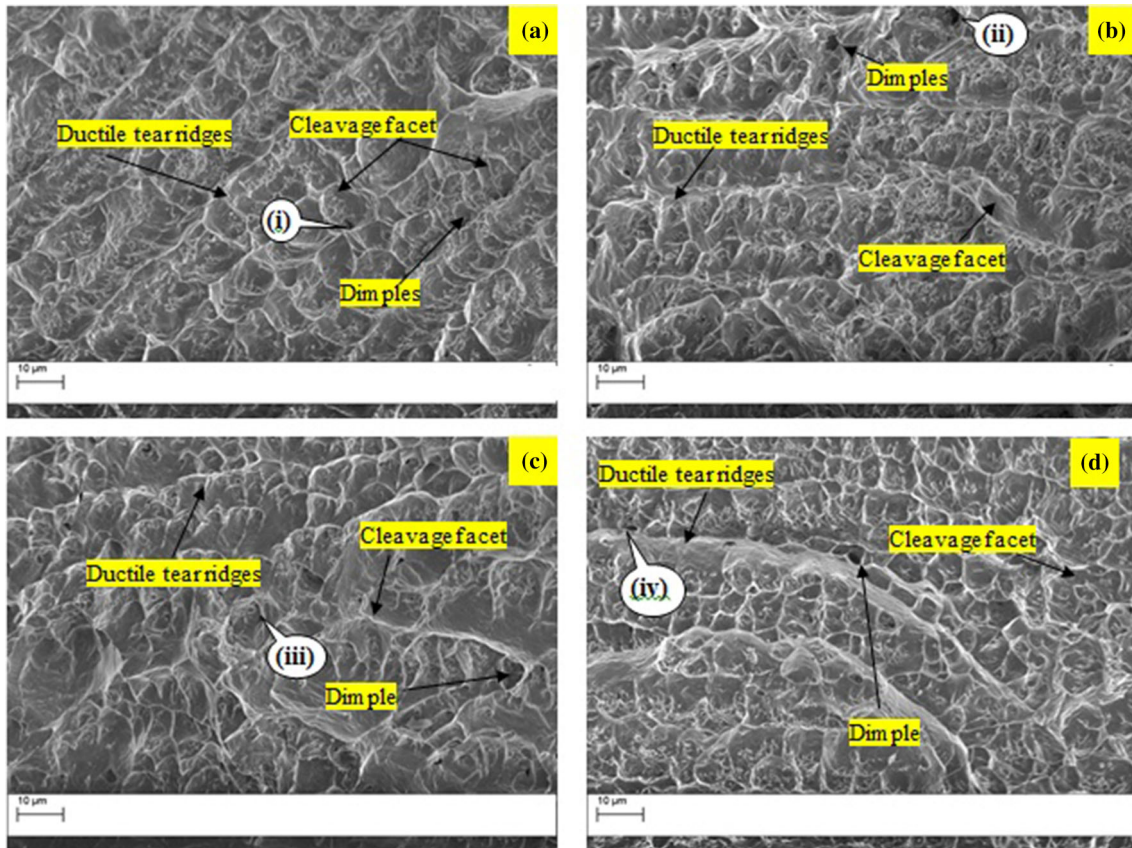
Fig. 13 Tensile failure—SEM fractography images of alloy C-2000 weldments made by (a) CCGTAW-filler-4 (b) PCGTAW-filler-4 (c) CCGTAW-filler-17 (d) PCGTAW-filler-17
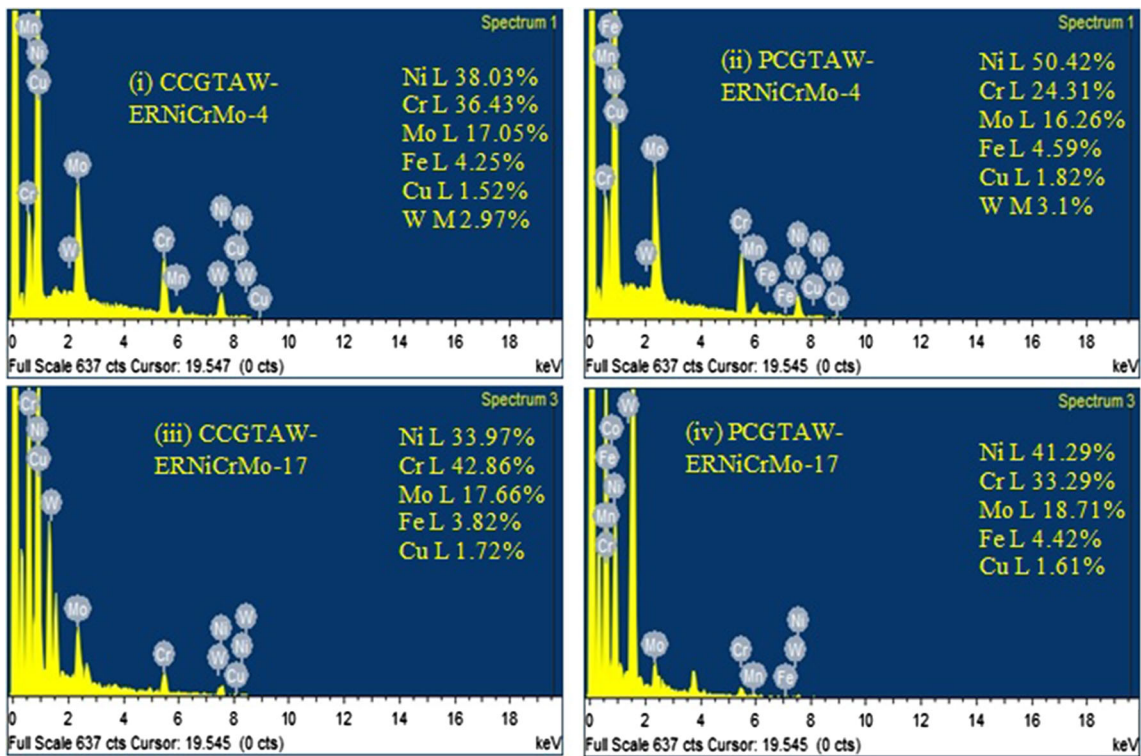

Fig. 14 SEM-EDS fractography of tensile fractured specimens of alloy C-2000 weldments made by (a) CCGTAW-filler-4 (b) PCGTAW-filler-4 (c) CCGTAW-filler-17 (d) PCGTAW-filler-17

are the reasons for improving the impact strength when switched over from CCGTA to PCGTA welding in both the filler wires. The toughness of all the weld joints in this study is inferior to the base metal, which is owing to the formation of Cr-enriched secondary phase precipitates in the FZ, as reported by Dupont (Ref 6). SEM fractography (Fig. 16a–d) indicates the ductile fracture mode with the existence of micro-voids and dimples. The ruptured area shows a large number of ductile tearing ridges, ductile dimples, and smaller facets of cleavage that mainly support the ductile mode failure.

3.7 Hardness Measurement

The hardness results show (Table 12 and Fig. 17b) that the average FZ hardness of all weldments in this study is marginally larger hardness than the BM. While comparing the hardness, no noticeable variations could be observed between the weldments. Both filler wires supply additional alloy elements that activate solution strengthening effect, which results in marginally increased hardness than the base metal. Figure 17(b) indicates the highest FZ average hardness for the PCGTAW-filler-4 (234 HV) among other counterparts, and the variation of hardness is ($\sim$ 3% to 6%) superior. The refined grain structure and less microsegregation offer the highest hardness in PCGTAW-filler-4. Also, the augmentation in hardness is attributed to the inclusion of Mo and Cr, as reported by Ozgun et al. (Ref 30). More undulations (Fig. 17a)
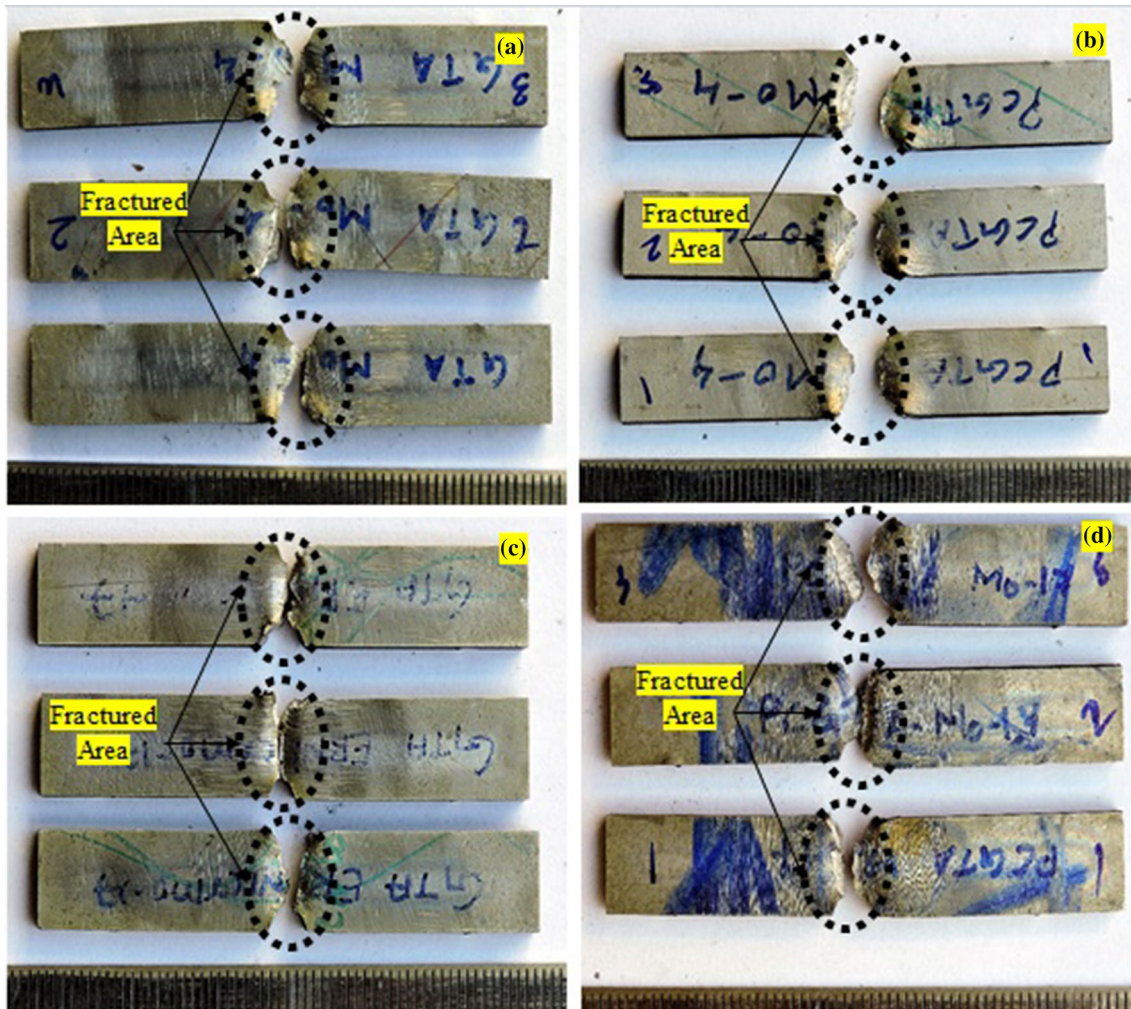
Table 11 Impact test results of alloy C-2000 weldments

Welding Method	Toughness, J	Mean Toughness, J
Base Metal	114.67	114.67
CCGTAW-Filler-4	58	57.33±3
	60	
	54	
PCGTAW-Filler-4	62	60.33±5
	54	
	65	
CCGTAW-Filler-17	54.6	55.46±0.75
	56	
	55.8	
PCGTAW-Filler-17	59	57.6±1.2
	57.2	
	56.6	

Fig. 15 Impact fractured samples of alloy C-2000 welds made by (a) CCGTAW-filler-4 (b) PCGTAW-filler-4 (c) CCGTAW-filler-17 (d) PCGTAW-filler-17
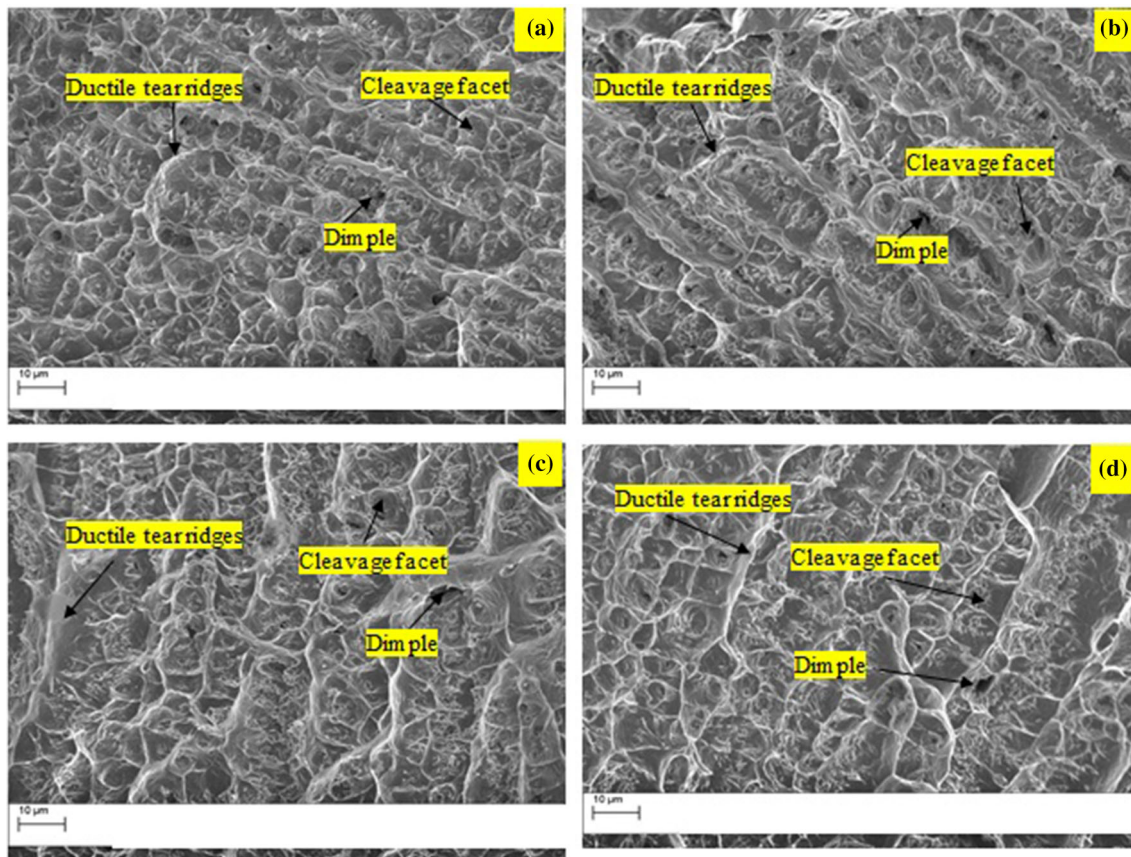
Fig. 16 SEM fractograph pictures of impact failure of alloy C-2000 welds made by (a) CCGTAW-filler-4 (b) PCGTAW-filler-4 (c) CCGTAW-filler-17 (d) PCGTAW-filler-17

Table 12 Hardness test results of alloy C-2000 weldments

Welding Process	Weld zone Average Hardness, (HV)	% augmentation with BM
Base Metal	220	.
CCGTAW-Filler-4	221±9.9	0.45%
PCGTAW-Filler-4	234±8.1	6.36%
CCGTAW-Filler-17	227±13.8	3.18%
PCGTAW-Filler-17	232±9.1	5.45%

were observed in the hardness profiles of both CCGTAW cases and PCGTAW-filler-17, which is because of the existence of secondary phases in higher fraction, and it is also proven by the SEM / EDS analysis.

3.8 Recommended Welding Technique

The current study recommends that weld joints produced by a current pulsing technique using ERNiCrMo-4 filler (i.e., filler-4) propose superior outcomes like improved microstructure features, lack of microsegregation and increased mechanical characteristics. Though it is not a matching filler wire of alloy C-2000, effective solubility of optimum alloying elements and higher amount of 'W' present in the filler wire (ERNiCrMo-4) increased the mechanical properties. It could therefore be preferred as most appropriate welding technique for most of the industrial application.

4. Conclusions

The conclusions of this experimental work are given as follows:

- Macro-investigation affirmed that the weldments employed in this study were defect free (no hot cracking, porosity and other discontinuity) and substantiated the adoption of suitable weld process parameters. Further it shows that weld bead profile controlling forces are well balanced.
- PCGTAW weld joints exhibit narrow bead width and small size HAZ which is owing to the efficient heat supply per unit volume at that time of current pulsation when compared with CCGTA welding.
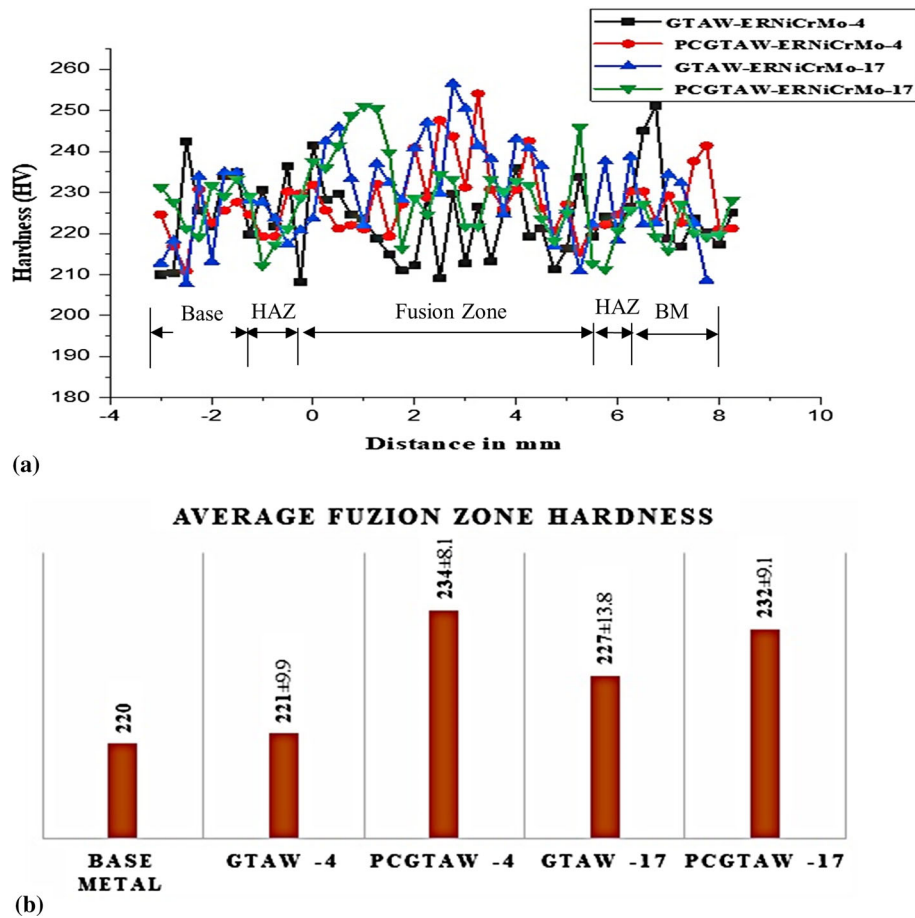- The PCGTAW microstructure (in both fillers) ended with fine equiaxed dendrites. Rapid cooling rate in PCGTA

Fig. 17 Hardness test results (a) Hardness profile (b) Average Fusion zone Hardness

welding primarily causes the microstructure refinement. However, for CCGTA welding, the microstructure of the FZ is characterized by coarser columnar dendrites.

- Analysis of SEM/EDS exposed the existence of secondary phases and larger microsegregation in CCGTA welding by using both fillers and PCGTAW-filler-17 filler. But it is significantly lesser in PCGTAW-filler-4 welds. Constant heat supply and inherent slow cooling rate in CCGTA welds resulted in severe microsegregation, which paved the way for higher volume of secondary phases.

- X-ray diffraction analysis proves that when shifting the welding mode from CCGTAW to PCGTAW, the overall reduction in grain size (grain refinement) in the PCGTA weld is 8.9 % for filler-4 and 9.77% for filler-17 cases.

- The results of the tensile, impact and hardness test show that PCGTAW-filler-4 weld joint has superior mechanical properties in terms of ultimate strength ($\sim$ 4% to 6%), ductility ($\sim$ 0.5% to 6.9 %), toughness ($\sim$ 5% to 7.5 %) and hardness ($\sim$3% to 6%) in comparison with other weldments employed in this study. Existence of fine equiaxed grains and less elemental segregation in microstructure was the reason for enhanced mechanical properties.

- The specific findings of the studies prove and suggest the usage of PCGTAW-ERNiCrMo-4 filler to join C-2000 alloy.

Conflict of interest

I confirm that there is no conflict of interest associated with the submission of this manuscript and that both authors have agreed its submission. Furthermore, the manuscript is original and has not been submitted to any other journal.

Ethical Approval

This article does not contain any studies with human or animal subjects

Reference

1. Technical Data Sheet https://super-metals.com/industrial-resources/nickel-chromium-molybdenum-alloy-hastelloy-c-2000-specialty-among-nickel-alloys/. Accessed 1 March 2019

2. Haynes International Technical Data Sheet http://haynesintl.com/docs/default-source/pdfs/new-alloy-brochures/corrosion-resistant-alloys/brochures/c2000.pdf?sfvrsn=e17929d4_20 2017. Accessed 14 August 2018

3. Technical Data Sheet https://super-metals.com/wp-content/uploads/2015/03/Hastelloy-C2000.pdf 2017. Accessed 14 August 2018

4. Technical Data Sheet https://www.parrinst.com/wp-content/uploads/downloads/2011/07/Parr_Hastelloy-C-2000-Alloy-Corrosion-Info.pdf. Accessed 25 December 2018

5. M. Manikandan, N. Arivazhagan, M. Nageswara Rao and G.M. Reddy, Improvement of Microstructure and Mechanical Behavior of Gas Tungsten Arc Weldments of Alloy C-276 by Current Pulsing, *Acta Metall Sinica*, 2015, **28**(2), p 208–215. (**in English**)

6. N. John Dupoint, C. John Lippold and D. Samuel Kiser, *Welding Metallurgy and Weldability of Nickel-Base Alloys*, 1st ed. Wiley, USA, 2009, p 19–72. (**in English**)

7. B. Arulmurugan, K. Modi, A.P. Sanjay, P.A. Yashwant, N. Rickwith, C.G. Mohan, P. Subramani, M. Agilan, M. Manikandan, N. Arivazhagan (2019) Effect of Post-Weld Heat Treatment on the Microstructure and Tensile Properties of Electron-Beam-Welded 21st Century Nickel-Based Super Alloy 686, Sådhanå, 44:38, pp. 1–10, (in English)

8. M.J. Cieslak, T.J. Headley and A.D. Romig, The Welding Metallurgy of Hastelloy Alloys C-4, C-22 and C-276, *Metall. Trans. A*, 1986, **17A**, p 2035–2047. (**in English**)

9. M. Raghavan, B.J. Berkowitz and J.C. Scanlon, Electron Microscopic Analysis of Heterogeneous Precipitates in Hastelloy C-276, *Metall. Trans. A*, 1982, **13**(6), p 979–984. (**in English**)

10. M.J. Cieslak, G.A. Knorovsky, T.J. Headley and A.D. Romig, The Use of New PHACOMP in Understanding the Solidification Microstructure of Nickel Base Alloy Weld Metal, *Metall. Trans. A*, 1986, **17**(12), p 2107–2116. (**in English**)

11. J.S. Ogborn, D.L. Olson and M.J. Cieslak, Influence of Solidification on the Microstructure Evolution of Nickel Base Weld Metal, *Mater. Sci. Eng. A*, 1995, **203**(1–2), p 134–139. (**in English**)

12. B. Arulmurugan and M. Manikandan, Improvement of Metallurgical and Mechanical Properties of Gas Tungsten Arc Weldments of Alloy 686 by Current Pulsing, *Trans. Indian Inst. Met.*, 2018, **71**(12), p 2953–2970. (**in English**)

13. C.C. Silva, R.M.C. Afonso, A.J. Ramirez, M.F. Motta, H.C. Miranda and J.P. Farias, Assessment of Microstructure of Alloy Inconel 686 Dissimilar Weld Claddings, *J. Alloys Compd.*, 2016, **684**, p 628–642. (**in English**)

14. M.D. Rowe, P. Crook and G.L. Hoback, Weldability of a Corrosion-Resistant Ni-Cr-Mo-Cu Alloy, *Weld. J.*, 2003, **82**(11), p 313–320. (**in English**)

15. A. John, K.J. Johny, B. Arulmurugan, S. Rajkumar, N. Arivazhagan, C.D. Naiju and M. Manikandan, Investigation on Microstructure and Mechanical Properties of Corrosion Resistance Alloy C-2000 Fabricated by Conventional Arc Welding Technique, *SAE Tech. Paper*, 2019 https://doi.org/10.4271/2019-28-0177

16. A. Srikanth and M. Manikandan, Development of Welding Technique to Avoid the Sensitization in the Alloy 600 by Conventional Gas Tungsten Arc Welding Method, *J. Manuf. Process*, 2017, **30**, p 452–466. (**in English**)

17. E. Farahani, M. Shamanian and F. Ashrafizadeh, A Comparative Study on Direct and Pulsed Current Gas Tungsten Arc Welding of Alloy 617, *MAE Int. J. Manuf. Mater. Sci.*, 2012, **2**(1), p 1–6. (**in English**)

18. M. Manikandan, N. Arivazhagan, M. Nageswara Rao and G.M. Reddy, Microstructure and Mechanical Properties of Alloy C-276 Weldments Fabricated by Continuous and Pulsed Current Gas Tungsten Arc Welding Techniques, *J. Manuf. Process.*, 2014, **16**(4), p 563–572. (**in English**)

19. B. Arulmurugan and M. Manikandan, Development of Welding Technology for Improving the Metallurgical and Mechanical Properties of 21st Century Nickel-Based Superalloy 686, *Mater. Sci. Eng. A*, 2017, **A69**, p 126–140. (**in English**)

20. F. George Vander Voort, *Metallography and Microstructures*, ASM Handbook, ASM International, Cleveland, 2004 (**in English**)

21. M. Sathishkumar and M. Manikandan, Preclusion of Carbide Precipitates in the Hastelloy X Weldment Using the Current Pulsing Technique, *J. Manuf. Process*, 2019, **45**, p 9–21. (**in English**)

22. H.R. Saedi and W. Unkel, Arc and Weld Pool Behavior for Pulsed Current GTAW, *Weld. J.*, 1988, **64**(11), p 247–255. (**in English**)

23. J.N. DuPont, Fundamentals of weld solidification, ASM handbook, *Welding fundamentals and processes*, Vol 6A, T. Lienert, T. Siewert, S. Babu, V. Acoff Ed., ASM International, Materials Park, OH, 2011, p 96–105. ((**in English**))

24. N. Karunakaran and V. Balasubramanian, Effect of Pulsed Current on Temperature Distribution, Weld Bead Profiles and Characteristics of Gas Tungsten Arc Welded Aluminum Alloy Joints, *Trans. Nonferrous Met. Soc. China*, 2010, **21**, p 278–286. (**in English**)

25. S. Kow, *A Textbook on Welding Metallurgy*, 2nd ed. Wiley, New Jersey, USA, 2003, p 170–194. (**in English**)

26. K. Mageshkumar, P. Kuppan and N. Arivazhagan, Characterization of Microstructure and Mechanical Properties of Nickel Based Superalloy 617 by Pulsed Current Gas Tungsten Arc Welding Technique, *Mater. Res. Express*, 2018, **5**, p 066541. (**in English**)

27. G.D. Janaki Ram, A. Venugopal Reddy, K. Prasad Rao and G. Madhusudhan Reddy, Control of Laves Phase in Inconel 718 GTA Welds with Current Pulsing, *Sci. Technol. Weld. Join.*, 2004, **2004**(9), p 390–398. (**in English**)

28. C. Pandey, N. Saini, M.M. Mahapatra et al., Study of the Fracture Surface Morphology of Impact and Tensile Tested Cast and Forged (C&F) Grade 91 Steel at Room Temperature for Different Heat Treatment Regimes, *Eng. Fail Anal.*, 2017, **71**, p 131–147. (**in English**)

29. P. Subramani and M. Manikandan, Development of Welding Technique to Suppress the Microsegregation in the Aerospace Grade Alloy 80A by Conventional Current Pulsing Technique, *J. Manuf. Process*, 2018, **34**, p 579–592. (**in English**)

30. O. Ozgun, H.O. Gulsoy, R. Yilmaz and F. Findik, Injection Molding of Nickel Based 625 Superalloy: Sintering, Heat Treatment, Microstructure and Mechanical Properties, *J. Alloys Compd.*, 2013, **546**, p 192–207. (**in English**)